Marine Biology (2022) 169:132
https://doi.org/10.1007/s00227-022-04120-0

ORIGINAL PAPER

The shell structure and chamber production cycle of the cephalopod *Spirula* (Coleoidea, Decabrachia)

Antonio G. Checa[1,2] · Christian Grenier[1] · Erika Griesshaber[3] · Wolfgang W. Schmahl[3] · Julyan H. E. Cartwright[2,4] · Carmen Salas[5] · Morgane Oudot[6]

Received: 19 May 2022 / Accepted: 26 September 2022 / Published online: 12 October 2022

Abstract

The endocochleate coleoid cephalopod *Spirula spirula*, the only present-day representative of the order Spirulida, secretes a coiled shell consisting of a series of chambers divided by septa and connected by a siphuncle. It is the shell closest to those of Recent and extinct ectochleate cephalopods: nautiloids, ammonoids. Therefore, its study may help to understand which characters remained unchanged or became transformed during the evolution of endocochleates. We have carried out detailed observations on the different structures composing the *Spirula* shell, with the aim of reconstructing their morphology, distribution, and mutual relationships. Alongside this, we also review the previous profuse terminology. Taking into account the additional information provided by growth lines and crystal orientations, we propose mechanisms for the secretion of the shell structures. All these mechanisms are integrated in a consistent way into a general model of chamber formation. The periostracum is secreted within a distinct periostracal groove. The outer shell layer is secreted externally to the periostracum by the soft tissues lining the shell externally. The inner shell layer is produced by the shell wall mantle, whereas the septa and the siphuncle are made periodically by a differentiated septal/siphuncular mantle. The most adoral septal mantle edge changes from secreting septal to inner shell wall material to produce the mural flap. The adapical ridge is formed by passive precipitates from cameral fluid residues trapped by surface tension, whereas the fibrous prismatic deposits of the connecting ring are biominerals produced remotely within mantle secretions. Homologies with *Nautilus* and *Sepia* are discussed.

Keywords *Spirula* · Shell · Chamber formation · Septum · Siphuncle · Microstructure

Introduction

The coleoid cephalopod *Spirula spirula* is the only present-day representative of the order Spirulida, belonging to the superorder Decabrachia that also includes cuttlefishes and squids. It is included in the subclass Coleoidea, together with the superorder Octobrachia (octopuses and vampire squids), all characterized by having very reduced or absent internal shells. While the earliest coleoids are recorded in the Early Carboniferous (Klug et al. 2019), the Spirulida (the initial representatives of the Decabrachia) did not appear until the Late Cretaceous (Fuchs et al. 2012). They are most likely linked to the order Belemnitida, which became extinct at the end of the Cretaceous (Fuchs et al. 2013). Together with the sepioids, *Spirula* is the only extant coleoid bearing a phragmocone consisting of a series of chambers separated by septa (Fig. 1a). While the *Sepia* cuttlebone is a highly modified phragmocone, the *Spirula* shell retains some characteristics shared—plesiomorphic—with ectocochleate

Responsible Editor: R. Villanueva.

✉ Erika Griesshaber
e.griesshaber@lrz.uni-muenchen.de

1 Departamento de Estratigrafía y Paleontología, Universidad de Granada, Granada, Spain

2 Instituto Andaluz de Ciencias de la Tierra, CSIC-Universidad de Granada, 18100 Armilla, Spain

3 Department für Geo- und Umweltwissenschaften, Ludwig-Maximilians Universität München, 80333 Munich, Germany

4 Instituto Carlos I de Física Teórica y Computacional, Universidad de Granada, 18071 Granada, Spain

5 Departamento de Biología Animal, Facultad de Ciencias, Universidad de Málaga, 29071 Málaga, Spain

6 UMR CNRS 6282 Biogeosciences, University of Burgundy-Franche-Comté, 21000 Dijon, France

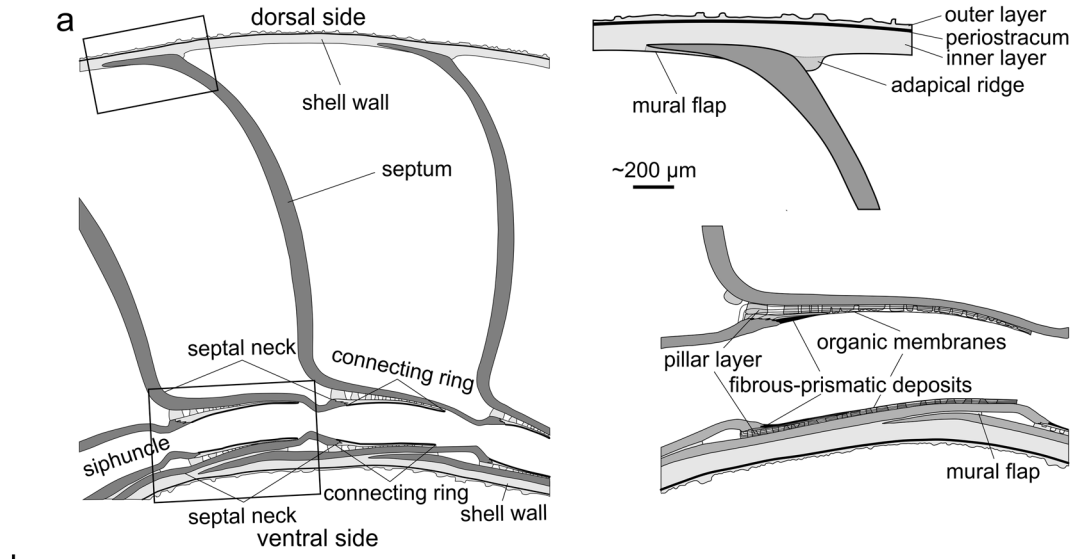

b

	Apellöf (1893)	Mutvei (1964)		Mutvei (1997)	Mutvei (2016)	Bandel & Boletzky (1979)	Doguzhaeva (1996, 2000)		This work	
Shell wall	Äussere Platte	Outer layer		Not studied	Not studied	Outer layer	Outer layer		Outer layer	
		Periostracum?				Central layer	Periostracum?		Periostracum	
	Innenplatte	Inner layer				Inner layer			Inner layer	
							Mural flap		Mural flap	
	Ausfüllungssunstanz des vorderen Kammerwinkel	Annular supraseptal ridge				Coarsely prismatic inner rim	Mural ridge		Adapical ridge*	
Septum									Septum	
Siphuncle	Sifonal-Düte	Septal neck	Septal neck						Septal neck	
	Pfeilerchen im Sifo		Semi-prismatic layer	Inner prismatic layer	Pillar layer	Pillar zone	Connecting ring	Spherulitic prismatic layer	Connecting ring	Pillar layer
	Sifonal-Hülle	Connecting ring	Chitinous layer	Not recognized	Chitinous layer	Conchiolin layer		Organic layer		Organic membranes
			Crystal cover	Spherulitic prismatic layer	Spherulitic prismatic layer	Not recognized		Not recognized		Fibrous prismatic deposits

Fig. 1 Main shell structures of *Spirula*. **a** Sketches of the structures distinguished within the shell and terminology applied to them in this study. **b** Terminology applied to the different shell structures in the literature and equivalence with the terminology of the present study. *adopted from Fuchs et al. (2012)

cephalopods (nautiloids, ammonoids) and their belemnoid ancestors: a phragmocone divided by a series of adorally concave septa traversed by a siphuncular tube in a ventral position. These plesiomorphies have made the *Spirula* shell, despite its rarity, the focus of many studies dealing with the structure and organization of the shell wall, septa, and siphuncle. The *Spirula* shell coiling is secondary (endogastric condition) and is contrary to that of coiled ectocochleates (exogastric coiling). Other characteristics constitute apomorphies of the Spirulida (Fuchs et al. 2013), including the septal microstructure, which was nacreous in nautiloids, ammonoids, and belemnitids, but consists of the so-called lamello-fibrillar microstructure in *Spirula*.

The first account of the morphology and the structures associated with the shell and septa of *Spirula* was provided by Apellöff (1893), who established the presence of two layers in the shell wall (outer and inner), the existence of a distinct deposit between the apical side of the dorsal

septal area and the shell wall, the adapical ridge ("Ausfüllungssubstanz des vorderen Kammerwinkel"), and the two main structures of the siphuncle, the septal neck and the connecting ring ("Sifonal-Düte", "Sifonal-Hülle"), as well as the siphonal pillars between the septal neck and the connecting ring of the next septum ("Pfeilerchen im Sifo") (Fig. 1b). Bøggild (1930) observed that the outer part of the shell wall was homogeneous, while the inner shell wall was made of 'rather regular prisms'. According to him, the septa were nacreous. Grégoire (1961) was the first to make electron microscope observations and noted the difference between the septal nacres of *Spirula* and *Nautilus*, the first one lacking typical tabular crystals. In his extensive study, Mutvei (1964) recognized and renamed Apellöff's structures, and made clarifications as to the structure of the shell wall and septa. In the shell wall, besides the two layers, which he called semi-prismatic, consisting of spicular crystalline elements, he recognized a middle organic (putatively periostracal) layer. In relation to the septum, he distinguished a conchiolin layer covering the convex apical septal surface and defined the 'annular supraseptal ridge' as being spherulitic-prismatic in nature. The connecting ring was composed of a 'conchiolin' layer lined externally by a spherulitic-prismatic layer. He renamed the siphuncular pillars of Apellöff (1893) as a semi-prismatic layer. This was later named pillar zone by Bandel and Boletzky (1979), and pillar layer by Mutvei (2016). Although Mutvei (1964) retained the term nacre for the material forming the septum of *Spirula*, he recognized the difference with the typically tabular nacre of *Nautilus*. Given the different aspect of the material forming the *Spirula* septum, Erben (1972) suggested the term lamello-fibrillar, which has been retained up to present day.

Later studies either conducted general reviews (Barskov 1973; Dauphin 1976, 1977; Bandel and Boletzky 1979) or focused on the structure of either the siphuncular tube (Mutvei 1997, 2016; Doguzhaeva 1996, 2000; Mutvei and Donovan 2006; Bandel and Stinnesbeck 2006) or the dorsal shell area (Oudot et al. 2020), mainly based on scanning electron microscope (SEM) observations. Although these refined some observations, they did not significantly alter the Apellöff/Mutvei model, with the exception of Doguzhaeva (1996, 2000) who noted the existence of a thin wedge of shell-wall-like material between the adoral prolongation of the septum and the inner shell wall, the mural flap. This structure was recognized by Fuchs (2006), Lemanis et al. (2020), and Oudot et al. (2020). In this way, the dorsal part of the septum is seen to be inserted within, rather than attached to, the inner shell wall.

The structures presently recognized in the shell of *Spirula*, together with the nomenclature we apply here, are sketched in Fig. 1a. The equivalences to the terms applied in the literature and in this study can be found in Fig. 1b.

The many studies on *Spirula* mainly aimed at describing the repertoire of structures within the *Spirula* shell. Even so, there is still some lack of information, because most of the studies were done either with optical microscopy (e.g. Apellöff 1893; Mutvei 1964) or with relatively low resolution SEM (e.g. Bandel and Boletzky 1979). With the exception of Mutvei (1964), who proposed a simple growth model of the adapical ridge, no previous study has focused on how the structures are secreted. Hence, it is not surprising that previous authors have paid little attention to those features that are basic for this purpose. Any growth model must take into account the positions of the mantle at different growth stages, that is, the distribution of growth lines. Determination of crystal orientation is also useful information, because when the crystals attain prismatic habits they orient their elongation axes perpendicular to the growth front, i.e. the mantle surface (Ubukata 1994; Checa and Rodríguez-Navarro 2001; Griesshaber et al. 2022). For understanding shell formation and growth, two complementary studies have been performed. Griesshaber et al. (2022) present measured crystal assemblies that characterize the main structural elements of *Spirula* phragmocones. In the present contribution, we review in great detail the different structures that comprise the *Spirula* shell, and their mutual relationships with optical and electron microscopy, and different preparation protocols. Based on the information provided by the additional abovementioned features (growth lines, crystal orientation), we provide growth models for them. As a corollary, we propose a model for the chamber formation cycle.

Materials and methods

Materials

Eleven dry shells were used for our study. Five of them were collected in Cacela Velha (Algarve, S. Portugal), one in Las Canteras beach (Las Palmas de Gran Canaria, The Canary Islands, Spain), two in Famara beach, and Caleta del Mojón Blanco (Lanzarote, The Canary Islands, Spain), and three in an unknown locality. Two additional specimens with the soft parts preserved in 70% ethanol were provided by the Centro Oceanográfico de Canarias (Santa Cruz de Tenerife, The Canary Islands, Spain). These specimens came from waters off Tenerife; unfortunately, their shells had become completely decalcified due to the long preservation time.

Optical microscopy

Three specimens were embedded in polyester resin (Vosschemie GTS) and cut approximately parallel to the coiling (symmetry) plane. Sections were thinned down with silicon carbide powder to transparency (~ 30 µm) and photographed

with a Leica DM1000 LED optical microscope, equipped with a Leica DFC295 camera, belonging to the Department of Stratigraphy and Paleontology of the University of Granada (UGR), Spain. The two specimens with the soft parts were dehydrated and embedded in methacrylate-based resin (Technovit 7200 VLC) in five steps. The first three steps were mixtures of ethanol (Et) and increasing proportions of Technovit (T) (30T/70Et, 50T/50Et, 70T/30Et) and the last two steps consisted of only Technovit 7200 VLC. The samples were subsequently polymerized. The embedded tissues were sectioned approximately parallel to the symmetry plane to a thickness of 50 µm using the cutting band system EXAKT 300CL. The sections were ground with a precision microgrinding system EXAKT 400C, and stained with toluidine blue. The entire process was carried out in the Andalusian Centre of Nanomedicine and Biotechnology (BIONAND, Málaga, Spain). Images were acquired with an Olympus VS120 optical microscope of the Central Services for Research Support (SCAI) of the University of Málaga (Spain).

Electron scanning microscopy (SEM)

One specimen was embedded in epoxy resin (EpoFix, Struers) and was cut along the equatorial plane (IsoMet 1000 precision cutter, Buehler). The surface was ground in successive steps with electroplated diamond discs (360, 600, 1200, and 3000 ANSI/CAMI US grit number) and subsequently polished with high-density wool felt pads, adding first 1 µm and then 0.25 µm of polycrystalline diamond suspension (Struers), until reaching a mirror-like finish (Hi-Tech Diamond polishing machine, All-U-Need model). The specimen was observed just after polishing and later, after etching with EDTA (1% wt) for one minute. Another shell was embedded in LR White resin (Fluka). The equatorial section was mirror-polished with 0.05 µm aluminum oxide paste and slightly etched with EDTA (1% wt) for 2 min. Three other specimens were broken and fragments of different areas of the shells were mounted and observed with SEM. Some fragments were cleaned with commercial bleach (~5% active chlorine) for 4–5 min or completely decalcified with 4% EDTA. The same thin sections used for optical micrography were polished with 0.5 µm grain size silicon carbide and etched with 4% EDTA for 1–2 min.

All specimens were mounted, carbon-coated (Emitech K975X carbon evaporator), and observed in either a Variable Pressure SEM Zeiss LEO 1430-VP, a field emission SEM Zeiss Auriga, or an FEI QemScan 650 F of the Center for Scientific Instrumentation (CIC) of the University of Granada (UGR), Spain, or a JEOL JSM-IT 100 InTouchScope (Univ. Burgundy, Dijon, France). Additional observations were made in a Phenom XL G2 Desktop SEM (Thermofisher) of the UGR (Excellency Unit UCE-PP2016-05) equipped with an Energy-dispersive X-ray spectroscopy (EDS) detector. Some EDS analyses were performed at an acceleration voltage of 15 kV, with a total of 11,103,226 counts in 6 min 34 s (28,128 c/s).

Transmission electron microscopy (TEM)

Wholly decalcified (4% EDTA) fragments of the central part of the septum were CO_2-critical-point dried (Polaron CPD 7501), post-fixed in OsO_4 (2%) for 2 h at 4 °C, and embedded in epoxy resin Epon 812 (EMS). They were sectioned with an ultramicrotome (LEICA Ultracut R) and prepared following standard procedures. Ultra-thin sections (50 nm) were stained with uranyl acetate (1%) followed by lead citrate. They were later carbon-coated (Emitech K975X carbon evaporator) and observed with a TEM Zeiss Libra 120 Plus. All the equipment is housed in the CIC (UGR).

Results

The *Spirula* shell is made by the elements considered above: shell wall, septum, and siphuncle (Fig. 1). In living specimens, the soft parts surround the outer shell surface throughout, including the areas between whorls, which have disjunct coiling (Fig. 2a, b). The soft parts also occupy the shallow living chamber and the siphuncular tube to the earliest chambers and the caecum.

Shell wall

The SEM observations allow us to observe the three layers differentiated by Mutvei (1964): outer and inner aragonitic, and middle organic (Fig. 3a). The outer layer forms the external ornamentation of the shell in the form of isolated and fused tubercles and more complex forms, defined as graphic pegmatite-like morphologies by Dauphin (1976) (Fig. 3b). The overall morphology and distribution of this ornamentation onto complete specimens were provided with micro-CT by Hoffmann et al. (2018). In section, these features appear as elevations with rounded to square outlines (Fig. 3a, c–i). The outer layer begins to form some way back (~5–10°) from the aperture (see also Hoffmann et al. 2018), where the inner layer is at its thickest (Fig. 3a, l). The thickness ratio becomes reversed toward the inner whorls: the outer layer thickens, at the same time that the inner layer thins (Fig. 3a, c–e), reaching exceedingly small values in the initial chamber (~1 µm in the example shown in Fig. 3e). The height of some of the outer tubercles reaches maximal values around one third of a whorl back from the aperture (Fig. 3c, h, i). With the increase in thickness of the outer layer, the reliefs become leveled off toward inner whorls, where their magnitude becomes minimal (Fig. 3d, e). These

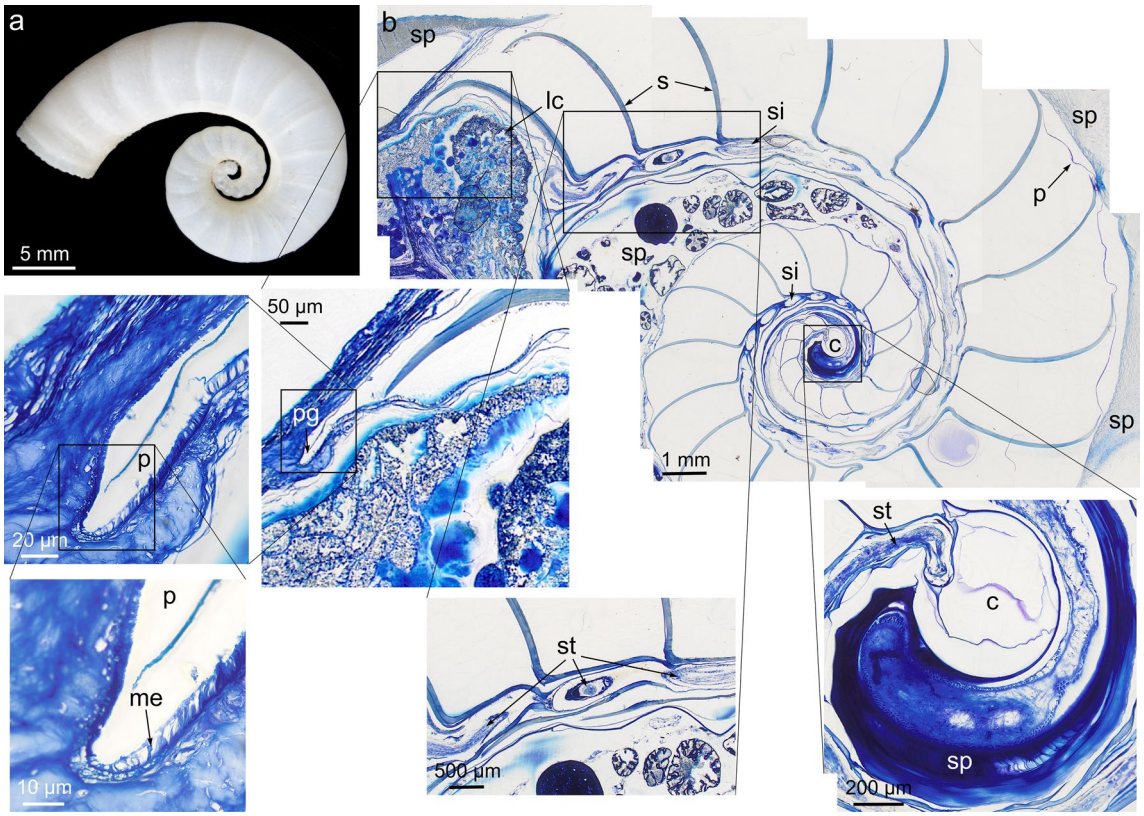

Fig. 2 Morphology of the *Spirula* shell and its relation with the soft parts. **a** External view of a large shell. **b** Section (composite image) of a methacrylate-embedded specimen with soft parts. It may correspond to an adult animal judging from the approximation of the last two septa (see Hoffmann et al. 2015 for evidence of maturity). The shell became decalcified due to a long time in ethanol. The soft parts surround the shell throughout and completely fill in the shallow living chamber, and the siphuncle up to the most internal chambers. The close-ups show both the insertion of the periostracum within the periostracal groove (note the single-celled mantle epithelium), and the presence of soft tissue all along the siphuncle up to the caecum. *c* caecum, *lc* living chamber, *me* mantle epithelium, *p* periostracum, *pg* periostracal groove, *s* septum, *si* siphuncle, *sp* soft parts, *st* siphuncular tissue

changes in thickness and ornamentation apply to the shell layers of both the dorsal and ventral areas.

On polished-etched sections, the crystals making up the two aragonitic layers are different. The crystals of the outer layer are, in general, much smaller in diameter (< 1 µm) than those of the inner layer, and can be qualified as fibrous (Fig. 3f, g). They are perpendicular to the shell wall. The fibrous layer is traversed by growth lines with outlines that usually change their shape during growth (Fig. 3a, c, d, f, h, i). This indicates that the features of the outer shell surface are not permanent and can change their morphologies and positions during growth.

The crystals of the inner layer have diameters from 2 to > 10 µm close to the contact with the organic layer, and are somewhat wider on average (up to 20 µm in diameter) at the internal shell surface (Fig. 3a, c, d, k). They can be defined as prisms. Their outlines are highly irregular, far from regular polygonal (Fig. 3e, j). Away from the intermediate organic layer of the shell wall, their outlines become diffuse (Fig. 3a, c, d, f, k, l, n). They become more recognizable again close to the internal shell surface. Their growth surface is even, except for some instances where, close to the next septum in the adoral direction, the ends of the individual prisms appear convex toward the shell interior (Fig. 3k).

Growth lines within the inner layer can be discerned with optical microscopy (Fig. 4) and, more rarely, with SEM (Fig. 3l, m). Within this layer, the growth lines run toward the central organic layer at a very low angle, estimated at 6–9°, both in the dorsal and in the ventral shell walls. These observations coincide with those of Mutvei (1964) and Doguzhaeva (2000).

The middle organic layer of the outer shell wall is relatively thin (5–7 µm in a medium-sized specimen), and thinly laminated (Fig. 3n). In a methacrylate-embedded decalcified specimen, the organic layer can be seen entering an invagination of the mantle margin (Fig. 2b). We can confidently identify both structures as the periostracum and the periostracal groove, respectively. The periostracal

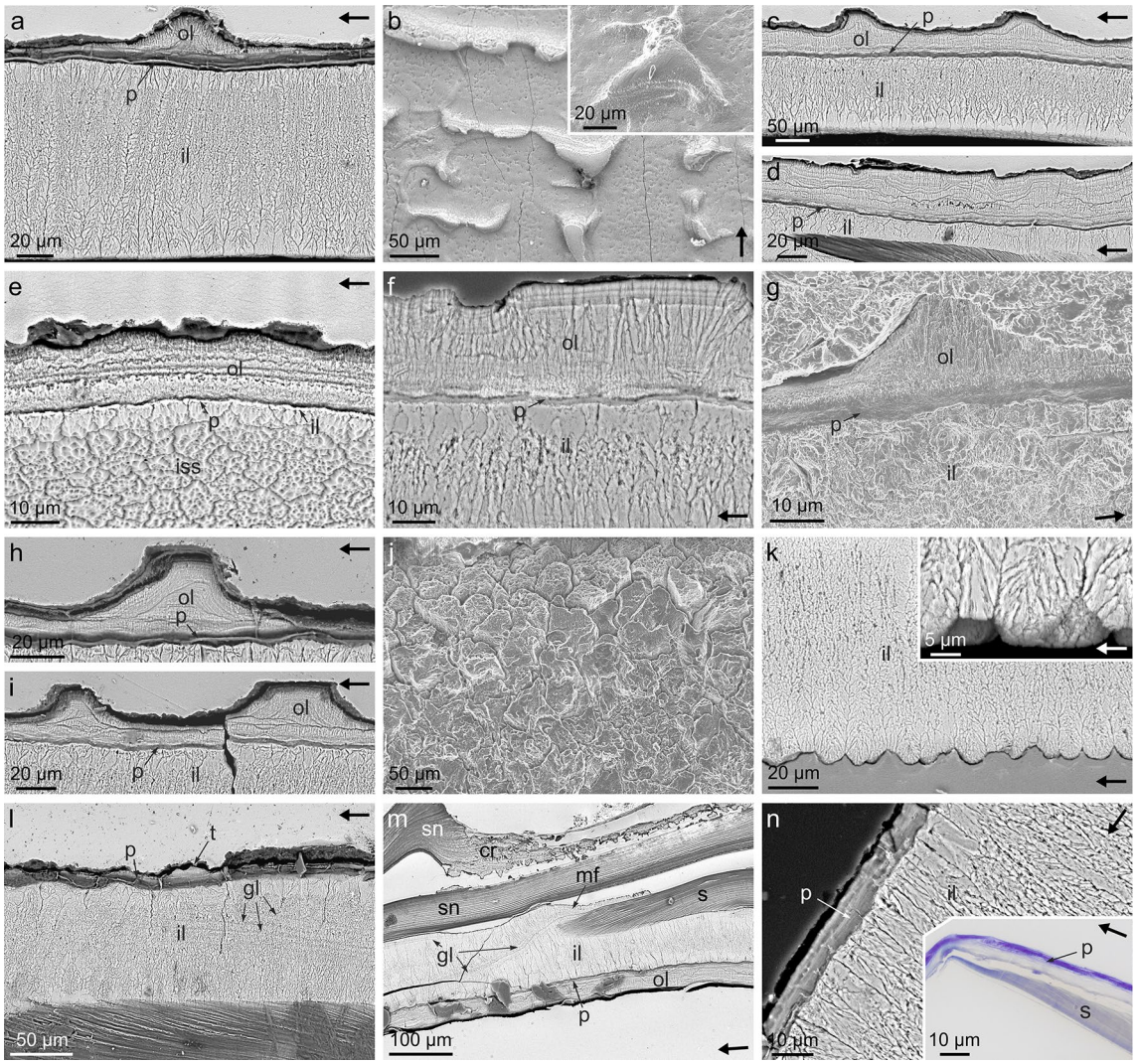

Fig. 3 Structure of the outer shell wall of *Spirula*. **a** Section through the dorsal shell wall besides the aperture. The outer shell layer is incipiently developed, whereas the inner layer reaches its maximum thickness. **b** Plan view of the outer shell surface decorated with reliefs with graphic pegmatitic outlines. Note growth increments at their slopes. The inset is a detail of another example. **c**–**e** Dorsal shell wall sections through progressively more internal positions. The thickness ratio between the outer and inner layers increases toward the inner whorls. **e** is a section of the initial chamber, where the thickness of the inner shell layer is exceedingly small; the complex polygonal outlines belong to the prisms of the inner shell wall on the internal shell surface. **f**, **g** Sections through the dorsal outer shell wall showing the orientation of the fibrous units of the outer layer perpendicular to the growth surface. Note the difference in thickness of the fibers of the outer shell layer and the prisms of the inner shell layer, as well as the noticeable growth lines in the former. **f** is a polished section whereas **g** is a polished/etched section. **h**, **i** Sections through the dorsal outer shell wall and part of the inner shell wall. The successions of growth lines give an idea of the changes in morphology and/or position of the reliefs of the outer shell layer. **j** View of the external surface of the prismatic inner layer (dorsal area). The outlines of the prisms are polygonal pseudodendritic. Note the similarity to the shapes in **e**. **k** Section through the internal part of the dorsal inner prismatic layer, close to the next septum. The growth surface is not flat, and every prism has a convex growth surface. **l** Section through the dorsal shell wall and final septum of an adult specimen. Marked growth lines are at a low angle to the surface. Note incipient outer shell layer and tubercle. **m** Section through the ventral area across the shell wall and three septa. Note growth lines in the shell wall in continuation with the septum edge. **n** Layered aspect of the periostracum in a shell section under the SEM and optical microscopy (inset). Arrows indicate the growth direction. *cr* connecting ring, *gl* growth line, *il* inner shell layer, *iss* internal shell surface, *mf* mural flap, *ol* outer shell layer, *p* periostracum, *s* septum, *sn* septal neck, *t* tubercle

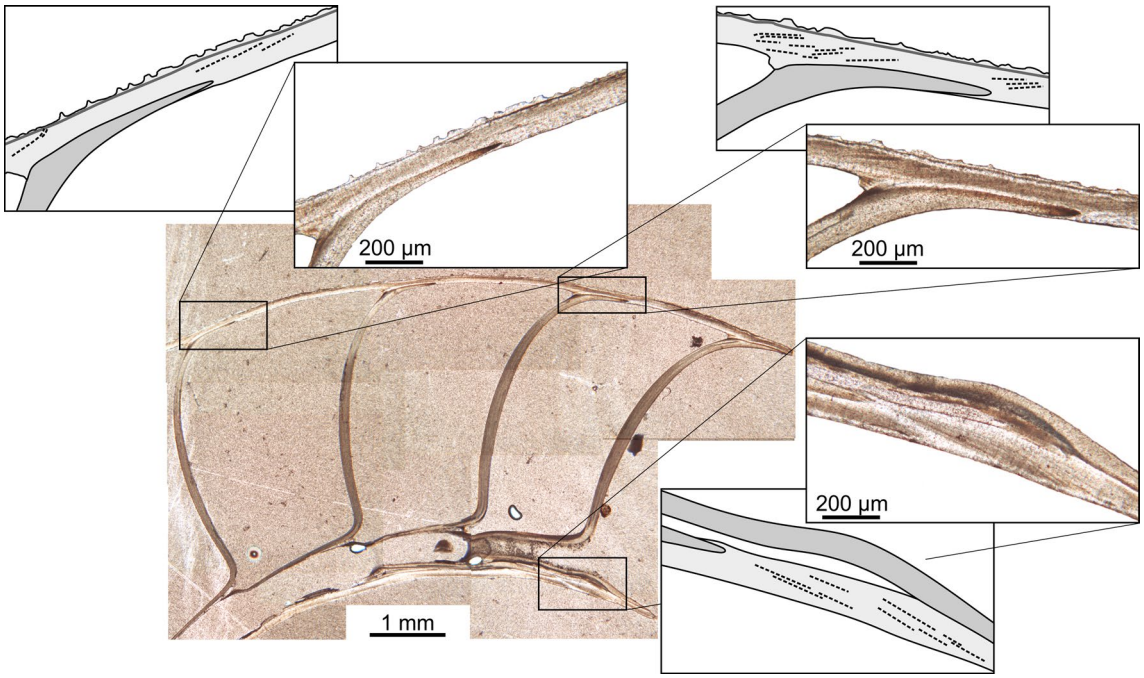

Fig. 4 Observation of the growth lines of the inner shell wall of *Spirula* in optical sections. The central image is a thin section through several chambers, and the close-ups are details of the dorsal (top) and ventral (bottom) areas. The distributions of the growth lines are shown in the corresponding sketches

nature of the middle organic layer was tentatively proposed by Mutvei (1964).

Septum and associated structures

Under the SEM, particularly under backscatter electron—BSE—mode, the septum displays a contrast different from that of the inner prismatic layer of the shell wall, due to its higher richness in organic matter (Fig. 5a, b). A similar contrast was observed by Hoffmann et al. (2018) with the micro-CT technique. It is a finely laminated structure, with the laminae parallel to the adoral and apical surfaces throughout (Fig. 5a, b), including the septal neck (Fig. 5c). In fracture, the laminae are made of fibers parallel to each other within each lamina and at high angles to those of adjacent laminae (Fig. 5d, e). Sometimes, short prismatic calcified layers are observed within the laminae (Fig. 5f). In plan view, the layers consist of short aragonite prisms extending perpendicular to the surfaces of the laminae (Fig. 5g). After decalcification, the septum retains its integrity and the fibrous aspect persists (Fig. 5h), which implies that the fibers are mainly organic. These can be discerned under the TEM, with individual thicknesses between 15 and 20 nm (Fig. 5i).

In detail, the boundary between the shell wall and the septum is thin, but gradual, with a reduction of the integrity of the prismatic units of the shell wall and an increase in the density of the organic laminae of the septum (Fig. 5j). The dorsal septum edge curves in the adoral direction (Fig. 5a). This effect is not so marked in the ventral area, where the septum enters the shell wall more or less in parallel (Fig. 5b). Both edges take the form of a bevel (Figs. 4, 5a, b). Some growth lines can be seen extending from the tips of the septal edges into the shell wall (Figs. 3m, 5k inset). Both edges become fully integrated within the shell wall since they are underlain by a wedge of prismatic material from the inner shell layer, the mural flap (Doguzhaeva, 2000) (Figs. 1, 3m, 4, 5a, b, k). The ventral mural flap is noticeably more acute than the dorsal one (compare Fig. 5a, b). The prismatic units of the mural flap directly below the septum edge are small and there is a sudden increase in size in the direction toward the internal shell surface (Fig. 5a, k). In the adoral direction, just beyond the septum edge, the mural flap is continuous into the inner shell wall. In the third dimension, the boundary between the mural flap and the septum is wavy and irregular, with no fixed wavelength or amplitude (Fig. 5l).

The insertion of the apical side of the dorsal edge of the septum is at a high angle to the shell wall (Figs. 5a, 6a–c). The corner between the apical side of the dorsal septum and the outer shell wall is filled with a mineral ledge, the adapical ridge (Fig. 6a–f). The adapical ridge or any equivalent is absent at the septal insertion of the ventral side, where the septum meets the shell at a very low angle (Figs. 3m, 5b). The contact between the septum and the adapical ridge is not neat and there is always a series of widely spaced

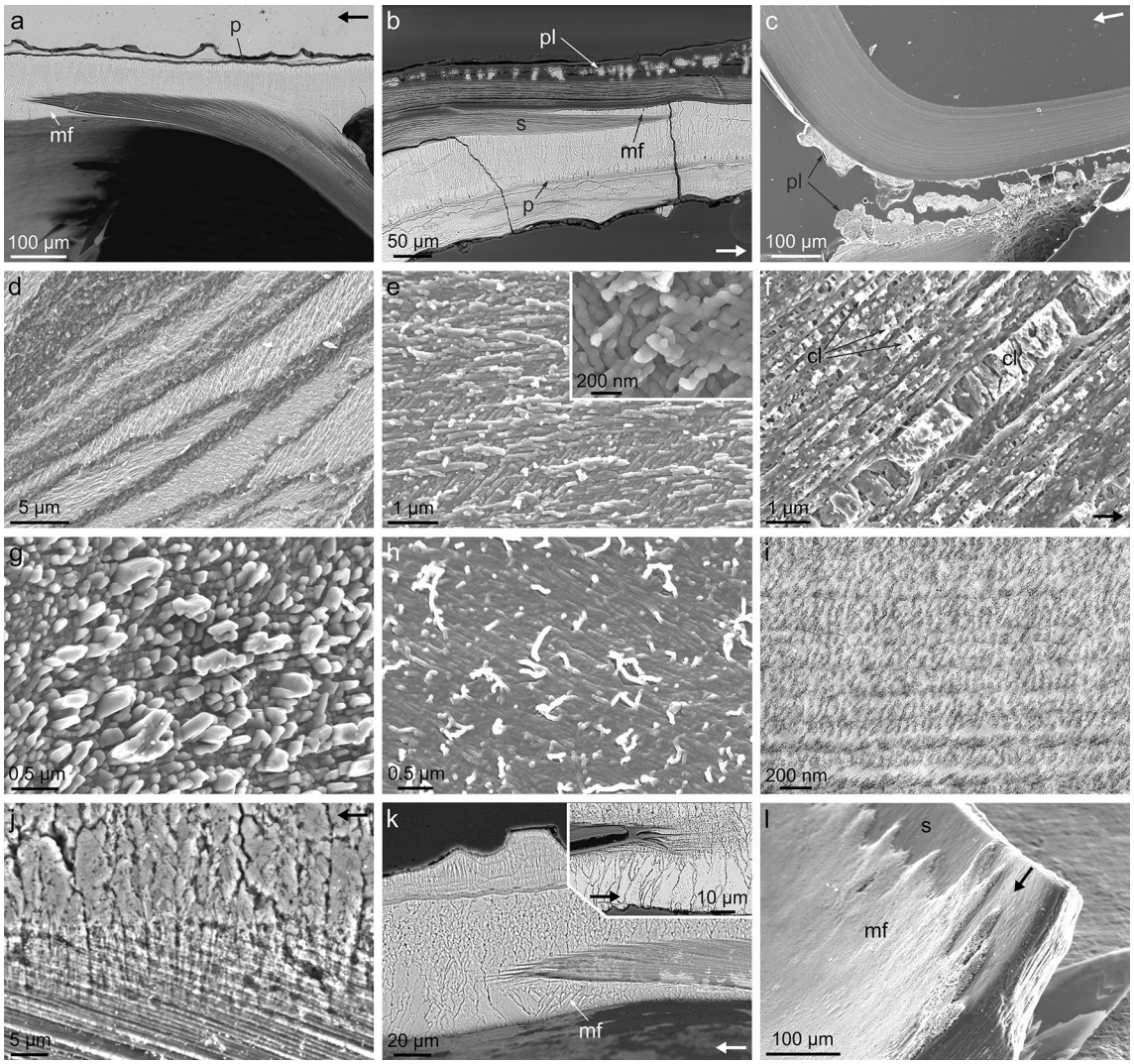

Fig. 5 Structure of the septum and associated structures in *Spirula*. **a** General view of the dorsal edge of a septum, showing the mode of insertion within the shell wall. **b** Mode of insertion of the septum within the shell wall in the ventral area. **c** Detail of the transition from the septum to the septal neck. The organic layers are strictly parallel to the outer and inner surfaces. The indicated pillar layer belongs to the next septum. **d** Oblique fracture through the septum. The laminae display a neat fibrosity, where the fibers are parallel within each lamina and differently oriented with respect to those of adjacent laminae. **e** View of two laminae distinguished by the different orientations of their constituent fibers. The inset is aimed at showing the dimensions of individual fibers. **f** Cross-section of the septum close to the dorsal area, showing the frequent intercalation of calcified laminae. **g** Surface view of a calcified lamina. It is made of short aragonitic prisms. **h** Decalcified septal surface. Despite some organic fibers having detached partly from the surface, the integrity of the septum is retained. **i** Slightly oblique TEM section of the decalcified septum. The different laminae and the individual fibers can be distinguished. **j** Transition between the inner shell wall and the septum in the dorsal area. The individual aragonitic prisms can be recognized across the initial organic laminae until they vanish completely within the septum interior. **k** Detail of the adoral end of the dorsal septal insertion. The mural flap is made of prisms identical to those of the inner shell layer. They initiate with small diameters, which soon increase drastically. The inset also shows organic laminae derived from the septum and vanishing within the inner shell layer. **l** Surface (oblique) view of the mural flap. The boundary with the septum is wavy and irregular. Arrows indicate the growth direction. *cl* calcified laminae, *mf* mural flap, *p* periostracum, *pl* pillar layer, *s* septum

organic laminae parallel to the rear septal surface included within the adapical ridge prior to the septum (Fig. 6a–d). Across the adapical ridge, in the adoral direction, we can observe a gradual increase in inclination from the shell wall-growth lines to the organic laminae of the adapical ridge and those of the septum (Fig. 6a–d). The same series of organic membranes can be observed in surface view (Fig. 6f). Of note, in section, the edge of the adapical ridge is irregular and changes between specimens and, within a single shell, from septum to septum. It is never homogenously curved and contains several curved segments of different sizes and shapes (Fig. 6a–e). The segments correspond to areas whose

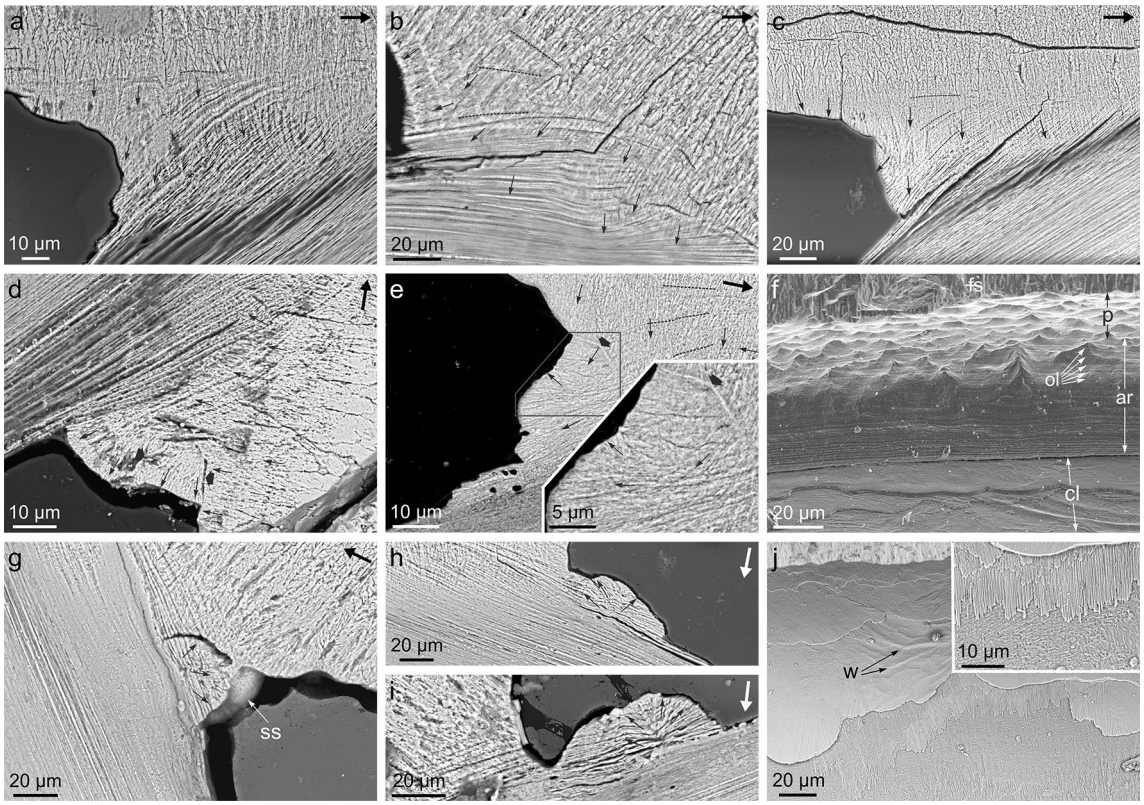

Fig. 6 Morphology and internal structure of the adapical ridge. **a–e** Sections through the adapical ridge. There is a progressive change in orientation from the growth lines of the shell wall to the organic laminae of the septum; some of them are indicated. The small arrows indicate the orientations of the mineral fibers. They are at high angles to the growth lines and to the organic laminae but can take a different orientation within the areas with convex outlines close to the edge of the adapical ridge. The thick short arrows in **d** and **e** indicate internal boundaries within such areas. **f** Surface view of the adapical ridge. The foreground shows prisms with convex terminations of the kind shown in Fig. 3k. Further in the background, organic laminae begin to appear. These become denser and denser until contact with the septal surface is reached. Some calcified layers extend onto the apical septal surface. **g–i** Sections through spherulitic structures developed at the boundary between the adapical ridge and the apical septal surface (**g**) or onto the septal surface (**h**, **i**). The internal distribution of mineral fibers is radial (arrows). Part of the external surface of the spherulite is visible in **g**. **j** Plan view of calcified layers extending onto the adoral septal surface. They are wrinkled in some areas and fibrous in nature, which is particularly visible in the inset. Arrows indicate the growth direction. *ar* adapical ridge, *cl* calcified layers, *fs* fracture surface, *p* prisms, *ol* organic laminae, *ss* spherulite surface, *w* wrinkles

boundaries are sometimes discernible (Fig. 6d, e). In section, the mineral material inside these structures is clearly fibrous, much thinner than the prisms of the inner shell wall (Fig. 6a–d). The fibers tend to orient at high angles to the external edge of the adapical ridge, whereas more toward the interior of the shell wall, the fibers coarsen and are at high angles to shell growth lines and the organic laminae above described, and change their curvature to adapt to the changing orientation of the laminae (Fig. 6a–e). In surface view, the convex segments correspond to rounded (spherulitic) or more continuous outgrowths (Fig. 6f).

Sometimes, laminar to convex structures extend onto the septal surface immediately ventral to the adapical ridge. They are traversed by the organic laminae extending from the adapical ridge (Fig. 6g–i). The aragonite fibers inside the rounded structures take on a radial, spherulite-like arrangement (Fig. 6g–i). In plan view, the laminar structures appear as superposed layers extending from the adapical ridge (Fig. 6f, j). They have irregular edges, are locally wrinkled and their surfaces display the fibrous nature typical of septal laminae (Fig. 6j and inset).

Siphuncular tube: septal neck and connecting ring

Every septum displays an apicalward tubular extension, called the septal neck, which, more toward the apex, transforms into the connecting ring (Fig. 7a). Close to the boundary, the septal neck develops a shallow constriction, after which its dorsal side coarsens (Fig. 7a). Immediately following this, the septal neck becomes wedge-like and transforms into the connecting ring (Fig. 7b). While the septal neck is a mere apicalward extension of the septum, the structure of the connecting ring is much more complex. At the contact area, the connecting ring consists of a series of very thin, loose

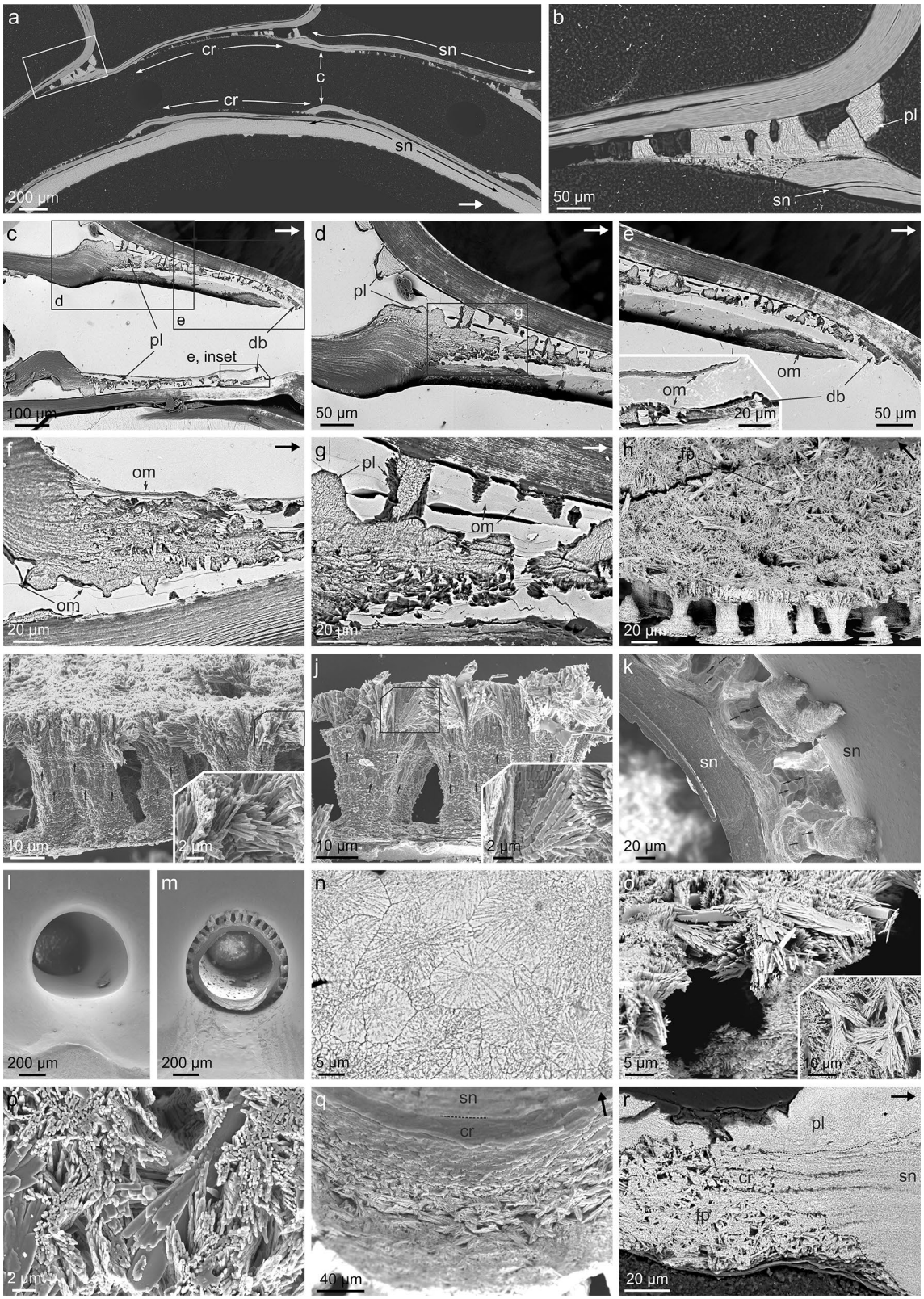

organic membranes that extend apically all along the septal neck extension (Fig. 7c–g). These are a continuation of those of the septal neck and may appear amalgamated due to surface tension (Fig. 7f, g). They become progressively more closely spaced toward the interior of the septal neck. These membranes coexist with two kinds of calcified structures:

◂**Fig. 7** Structure of the *Spirula* siphuncle. **a** General view of the siphuncle across several chambers. **b** Detail of the area framed in **a**, showing the contact between the septal neck and the connecting ring, delineated with a broken line. The pillar layer contains clearly discernible growth lines. **c** Complete view of the connecting ring. The venter is to the bottom. **d**, **e** Details of the areas framed in **c**, showing changes in the dimensions of the pillars and the position of the distal buttress. **f**, **g** Details of the ventral and dorsal connecting ring areas, respectively, close to the contact zone with the septal neck. **g** is a close-up of the area framed in **d**. The intercalation of the organic membranes and pillars is clear. Organic membranes become progressively more closely spaced toward the interior of the connecting ring. In **f**, the organic membranes of the connecting ring are continuous with those of the septal neck, and the most internal organic membranes (top of the image) are devoid of any calcification. **h** General view of the pillar layer with fibrous prismatic deposits on top (interior of the connecting ring). Some details of the pillars in the foreground are shown in three dimensions in Online Resource Fig. S1b and c. **i**, **j** Examples of pillars showing their feather-duster-like top part. The insets show the mode of splitting of fibers, leading to such morphologies. Small arrows indicate particular growth increments. **k** Pillars of the most adoral part of the pillar layer, attached to the septal necks of both their corresponding septum and the previous septum. Small arrows indicate particular growth increments. **l**, **m** Views of the adoral surfaces of the last-formed (**l**) and a previous septum (**m**) showing the aspect of the septal neck. Contrary to the previous septa (**m**), the last septum (**l**) is devoid of pillars. **n** Transversal cross-section across an area of coalescing pillars. Note polygonal outlines, differences in size, and internal fibrosity. **o**, **p** Fibrous-prismatic deposits on top of, i.e. internal to, the pillars. Note the difference in size and orientation with the top fibers of the pillars. The fibrous prismatic aggregates seem to grow within the interstices between pillar fibers. **q** View of the interior of the connecting ring in the adoral direction, with the septal neck in the background (boundary indicated). The fibrous prismatic deposits are denser and thicker in the direction to the septal neck. **r** Section through the contact between the septal neck and the connecting ring, showing the abundance of fibrous prismatic deposits. The approximate boundaries between septal neck, pillar layer, and fibrous prismatic deposits have been delineated with broken lines. Note continuous layering from the septal neck to the connecting ring. Arrows indicate the adoral direction. *c* constriction, *cr* connecting ring, *db* distal buttress, *fp* fibrous prismatic deposits, *om* organic membranes, *pl* pillar layer, *sn* septal neck

the pillar layer and the fibrous prismatic deposits. The pillar layer is made of pillar-like structures (Fig. 7h–k) which extend from the interior of the septal neck of the previous septum to the connecting ring, and all along the extension of the connecting ring (Fig. 7a–e). This layer is present within the interior of all septal necks, except for the last-formed septum in three complete specimens studied with both optical microscopy and SEM (Fig. 7l, m). Pillars have variable widths (10–30 µm) and sometimes fuse to form wider structures (Figs. 7h–j, Online Resource Fig. S1). They have wide initial bases, then narrow significantly (they rarely extinguish; Online Resource Fig. S1b) and later become cylindrical or more or less conical. Toward the interior of the connecting ring, they acquire a feather-duster-like morphology by progressively developing branches with lath-like profiles oriented radially (Figs. 7h–j, Online Resource Fig. S1), i.e. they transform into spherulites. This is due to the individual fibers branching repeatedly at increasing inclinations to the growth axis of the pillar (Fig. 7i inset, j inset). In longitudinal polished sections, there are closely spaced growth lines continuous across the pillar layer (Fig. 7b). Some of these growth increments, if not all, correspond to their intersection with the individual membranes of the connecting ring (Fig. 7f, g). In lateral view, the growth stages are marked by changes in diameter and/or texture and can be traced across different pillars (Fig. 7i–k). Upon coalescence, the cross-sections of the pillars are pseudo-polygonal and reveal their internal fibrosity (Fig. 7n). The maximal height of the pillars (40–50 µm) diminishes in the apical direction (Fig. 7c–e). There is also a height reduction from the dorsal to the ventral side (Fig. 7c). In the apical direction, the pillar layer ends in an elongated pillar with a final elevated tip, forming a kind of buttress, here called the distal buttress, for the attachment of the organic layers (Fig. 7c, e).

In addition to the pillars, there are fibrous prismatic deposits made by elongated crystals (1–5 µm in diameter) which frequently form more or less complete radial aggregates (Fig. 7o, p). Our EDX data indicate that their elemental composition is consistent with aragonite (Online Resource Fig. S2). They form dense aggregations close to the contact with the septal neck (Fig. 7q, r), whereas, in the apical direction, the crystal aggregates become more and more sparse (Fig. 7h, q). They may appear integrated within the fibers of the feather-duster-like top part of the pillars (from which they can be distinguished by their much bigger sizes) (Fig. 7h, o, p), although most frequently, they appear above, interleaved with the organic membranes (Fig. 7r). They do not seem to occupy the interstices of the most internal membranes (Fig. 7f).

Discussion

Shell structures and microstructures

Shell wall

Our study together with that of Griesshaber et al. (2022) demonstrates that the outer and inner shell layers are made of fibrous and prismatic aragonite, respectively, on the basis of the different diameters of the units and of the orientation of their long axes at a high angle to the shell surface. The prisms of the inner wall are characterized by being single crystals with irregular boundaries, both in longitudinal and transversal views. According to the microstructure glossary of Carter et al. (2012), this microstructure can be classified as 'irregular simple prismatic'. From here on, we disregard the equivocal term semi-prismatic usually employed (e.g. Mutvei 1964).

Both layers show bidirectional growth from the middle organic layer, which is undoubtedly the periostracum, as tentatively proposed by Mutvei (1964). This is fully supported by the identification of the periostracal groove from which the periostracum is extruded (Fig. 2b). Accordingly, the periostracum is the first layer to be secreted, and, shortly after, both the outer and inner shell layers begin to be secreted in the external and internal directions, respectively. In ectocochleate cephalopods, the periostracum is secreted by the internal surface of the outer mantle fold (OMF). At the tip of the OMF, the periostracum becomes reflected posteriorly and secretion of the shell layers begins below it. In *Spirula*, there is no distinction between the different mantle folds. We can homologize the mantle surface that secretes the periostracum, (which has a characteristic single-celled structure; Fig. 2b) and the inner layer of the shell wall with the OMF surface of *Nautilus* (Mutvei 1964) and molluscs, in general. The inner shell layer thickens steadily and soon reaches its maximum thickness immediately in front of the last-formed septum (Fig. 3a). The outer shell layer grows continuously and thickens in the apical direction. It must be secreted by the mantle enveloping the shell externally (Fig. 2b). The fine structure of the mantle and the rest of the soft parts should be studied further in a properly fixed specimen.

The recognition of growth lines in the outer shell layer in polished-etched sections under the SEM is relatively frequent (Fig. 3a–i). They show how the structures of the outer shell surface change their morphology and position. Growth lines in the inner layer could be recognized mainly in thin sections with optical microscopy (Fig. 4), but rarely under the SEM (Fig. 3l, m). They are always at a low angle (less than 10°) to the periostracal layer. Our observations coincide with those of Mutvei (1964, plates 16 and 18, fig. 1) and Doguzhaeva (1996, plate 4, fig. 2, 2000, plate 2, figs. 5, 6). Accordingly, at every growth stage, the inner margin seems to be an acute wedge. An apertural reinforcement in the adult shell was observed by Doguzhaeva (2000).

Septum and septal insertions into the shell wall

The septum has a lamello-fibrillar microstructure, a term proposed by Erben (1972), and defined by him as "an aragonitic, laminar, plywood-like shell microstructure consisting of sheets of more or less mutually parallel, horizontal fibers, with fiber orientations differing in successive laminae". This term, which we will adopt here, is also applied to the microstructures of Cambrian molluscs (Carter et al. 1990). In addition to the organic layers, there is some degree of mineralization, including the existence of thin calcified layers (Fig. 5f, g). This microstructure forms the septum from its insertion within the shell wall to the end of the septal neck. The organic layers later continue into the connecting ring (e.g. Figure 7f, g). The organic layers are parallel or subparallel to the septal surface (Fig. 5a, c, 7b). We can confidently assume that they correspond to growth increments. This is supported by the fact that the organic membranes of the dorsal septal edge curve adoralward to be continuous into the growth lines of the inner shell wall (Figs. 3l, m, 4).

The abrupt change between the septal material and the prisms of the mural flap (Figs. 3m, 5a, b, k) indicates that the two materials are made by the same mantle epithelium, which suddenly changes the mode of secretion. Otherwise, we find it impossible that a proper septal mantle becomes emplaced dorsalward to the position of the septal edge and later retracts completely when the mural flap is going to be secreted.

The succession of organic layers with alternating orientations of their constituent fibers (Fig. 5d, e), a species of twisted plywood, is typical of a liquid crystalline chiral nematic phase (Bouligand 1972; Neville 1993). This mechanism was proposed for the interlamellar membranes of molluscan nacre (Cartwright and Checa 2007), which in the nautilids and ammonoids makes up the septa, and for the organic phase of the septa and chambers of *Sepia* (Checa et al. 2015). Both materials are homologous to the septal organic membranes of *Spirula*. Accordingly, we propose that liquid crystallization is a general process for the formation of the organic matrix of the septa across cephalopods.

On the apical side of the dorsal septal edge, the production of septal material is predated by the production of loosely spaced membranes, which become denser and denser as the apical septal surface is approached (Fig. 6a–e). These membranes are parallel to those of the dorsal septal surface and are no doubt formed by the advancing septal mantle. These membranes indicate a progressive emplacement of the rear septal mantle to the position of the next septum, and their decreasing distance results from the decreasing speed of advance of the soft body. The curved membranes reflect the shape of the rear soft body, which coincides with the progressive inclination of the prisms of the inner shell layer to meet them at a high angle (Fig. 6a–d), since prismatic units always tend to grow at a high angle to the molluscan mantle growth surface (Ubukata 1994; Checa and Rodríguez-Navarro 2001).

The adapical ridge is the zone of transition from the inner layer to the septum, where there is a change from aragonite to organic secretion. If the adapical ridge material were produced by the mantle, its outline would be flat or gently curved and consistently shaped in the different samples analyzed. On the contrary, the different adapical ridges analyzed have irregular and changing edges (Fig. 6a–e), even within a single shell, and the constituent material is rather fibrous. Aragonite fibers orient at a high angle to the margin of the adapical ridge, more or less in continuation with the prisms of the inner shell wall (Fig. 6a–c, e). When spherulitic features are present (Fig. 6c–e), the mineral fibers

inside them are at high angles to their edges. Accordingly, we interpret that the material forming the adapical ridge is formed by secondary deposits precipitated remotely, out of contact with the mantle, which overgrow the previous mantle secretions. Mutvei (1964) showed similar granular and prismatic spherulitic deposits forming the adapical ridge of *Nautilus pompilius*. They were likewise formed by secondary precipitation. Figure 8 shows several examples where we have tentatively delineated the extension of these secondary deposits in *Spirula* on the basis of their fibrous aspect and the orientation of the fibers. These secondary deposits had to be formed when the septum was being formed or even finished. We hypothesize that they could have been produced in a late stage of cameral liquid emptying by residual cameral liquid trapped in this acute corner by surface tension. Similar remote precipitates are responsible for the flat and spherulitic deposits extending from the adapical ridge onto the apical dorsal septal surface (Fig. 6f–j), as well as for those instances of prisms with convex ends found close to the adapical ridge (Figs. 3k, 6f). Additional fibrous deposits of similar origin can sometimes be found in other areas of the chambers (Online Resource Fig. S3).

Mutvei (1964) defined three layers in the dorsal septal area: (1) conchiolin layer, (2) spherulitic-prismatic layer and (3) nacreous layer. We have not been able to recognize any obvious conchiolin layer, and his spherulitic-prismatic layer corresponds to the adapical ridge and adjacent deposits extending onto the septal surface. His nacre layer corresponds to the lamello-fibrillar septum.

Siphuncle

The siphuncle is constituted by two well-defined structures, the septal neck, and the connecting ring. The septal neck is a mere apicalward tubular extension septum (Fig. 7a). Our observations indicate that the connecting ring is formed by organic membranes, which become more densely spaced from the exterior to the interior (Fig. 7f, g). Their tendency to merge by surface tension upon dehydration probably led Mutvei (2016) to interpret this as a single (chitinous) layer. All organic membranes are a continuation of those of the septal neck, which cease to be mineralized at the transition septal neck-connecting ring. This indicates that the connecting ring is contemporaneous with the septal neck and hence, with the rest of the septum. Accordingly, the connecting ring grows centripetally, toward the interior.

The organic membranes of the connecting ring cross the pillars of the pillar layer externally (Fig. 7c–g), whereas

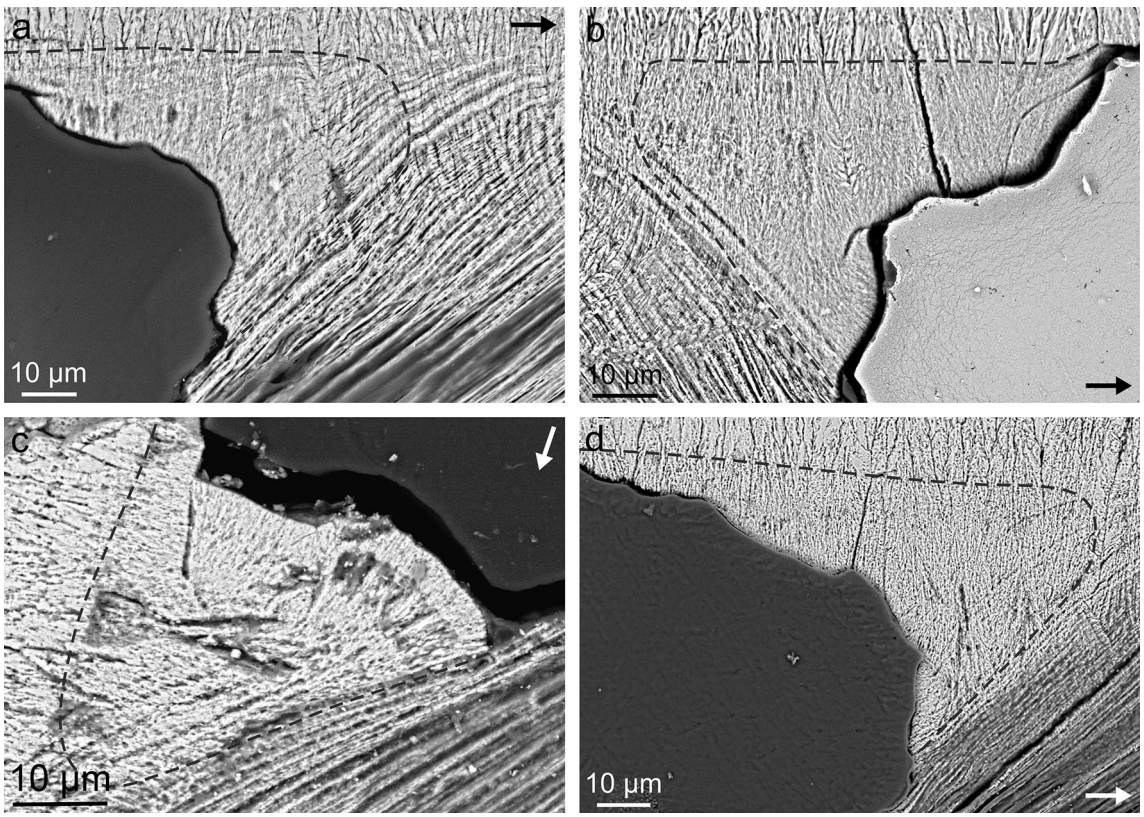

Fig. 8 **a–d** Sections across the adapical ridges on which the boundaries of the secondary deposits have been tentatively delineated (broken lines) on the basis of the fibrous aspect of the material and the orientation of the fibers. Arrows indicate the growth direction

more internally the fibrous prismatic deposits are intercalated within them (Fig. 7q, r). The pillar layer and the associated organic membranes are clearly the first deposits to be formed during the formation of the connecting ring. This layer is characterized by conspicuous growth increments, both in section and on the surfaces of the pillars (Fig. 7b, f, g, i–k). The pillars are perpendicular to the surfaces of the connecting ring and of the previous septal neck (Fig. 7k, m), which indicates growth perpendicular to both structures by the connecting ring mantle. In other words, the pillar layer has to be formed when the mantle is more or less stationary and must correspond to the initial stages of formation of the chamber to which the connecting ring belongs. This is supported by the fact that the last-formed septum never contains pillar deposits (Fig. 7l). This is also evident in Apellöff's (1893) illustration of the last septum of a specimen (his plate 9, fig. 2). Accordingly, it does not belong to the preceding septal neck, as was proposed by Mutvei (1964).

Toward the interior of the connecting ring, the first fibrous prismatic aggregates can be found integrated within the fibers of the feather-duster-like ends of the pillars (Fig. 7o, p). Here, they are consistently at a high angle to the axes of the pillars, and they seem to be mostly intercepted by the fibers of the feather-duster-like tops of the pillars. This indicates that they begin to grow during the last stages of, or after, pillar growth. They form dense accumulations internal to the pillars, mainly at the initiation of the connecting ring, close to the septal neck, where they grow between the organic membranes (as shown also by Mutvei 2016) (Fig. 7q, r). Shortly after, in the apical direction, they become progressively scattered and disappear (Fig. 7h, q). These aggregates were considered by Mutvei (1964, 1997, 2016) and Mutvei and Donovan (2006) to form a spherulitic-prismatic layer, but no trace of proper spherulitic structures has been observed. They form dense—close to the septal neck—to scattered—in the apical direction—aggregations, but cannot be considered a proper layer. Their orientations, at low angles to the organic membranes of the connecting ring, i.e. to the growth increments or to the secreting siphuncular mantle, indicate that they are not formed in contact with the connecting ring mantle. They are most likely remote deposits formed by mineralizing fluids around the proximal end of the connecting ring. We hypothesize that they may be formed within some kind of mineralizing extrapallial fluid (gel) exuded by the connecting ring mantle. Crystallization of fibrous prismatic deposits initiates after the mantle has abandoned their position. Their formation might reinforce the connecting ring.

Homology of the siphuncular structures with *Nautilus* and *Sepia*

The siphuncle of *Nautilus* is made of a septal neck and a connecting ring (Mutvei 1964, 1972). As in *Spirula*, the septal neck is an apicalward extension of the septum and consists of a septal nacre layer lined internally by a prismatic layer, in turn coated internally by a spherulitic-prismatic layer (Fig. 9). The images provided by Mutvei (1997) prove that the prismatic and the spherulitic-prismatic layers are microstructurally identical to the pillar layer and the fibrous prismatic deposits of the *Spirula* siphuncle. The former was in fact named pillar layer by Bandel and Boletzky (1979). The connecting ring consists of an outer spherulitic-prismatic layer and an inner organic layer (Mutvei 1972). The outer layer (called the chalky layer by Bandel and Boletzky 1979, and Bandel 1990) begins to be present on top of the apical end of the nacreous layer of the septal neck and is made of a material of fibrous prismatic type (Fig. 9). The inner organic layer (conchiolin layer of Mutvei 1972, or glycoprotein layer of Mutvei 1997) is adorally continuous with the nacreous layer of the septal neck and, according to the images in Mutvei et al. (2010), we interpret that it is made by

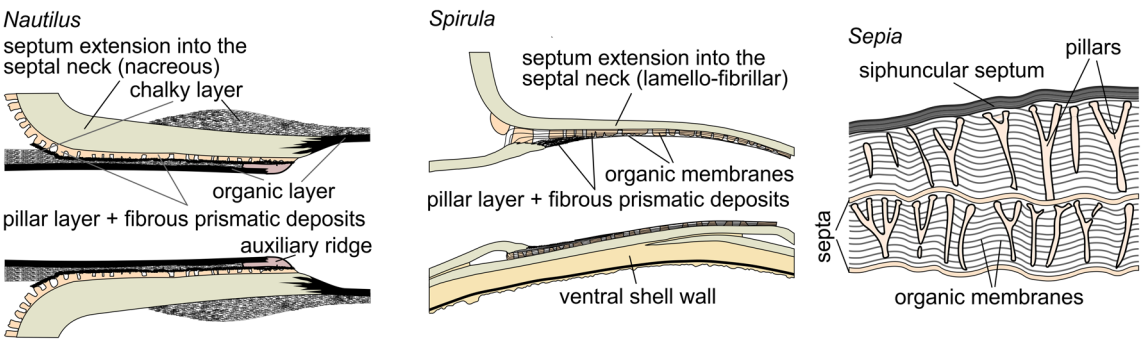

Fig. 9 Siphuncle structures of *Nautilus* and *Spirula*, and chamber and siphuncle structure of *Sepia*. The septum extensions into the septal necks, and their associated pillar layers and fibrous prismatic deposits of *Nautilus* and *Spirula* are homologous. The same applies to the organic layer and the organic membrane complex of the connecting rings of both genera. Conversely, no elements of the chambers and siphuncle of *Sepia* can unequivocally be homologized with siphuncular elements of *Nautilus* and *Spirula*. The sketch of *Nautilus* is modified from Mutvei (1972), and that of *Sepia*, from Checa et al. (2015). For *Spirula*, compare with e.g. Fig. 7a

the individual membranes left after the mineral component of the nacreous layer ceases to be secreted, in much the same way as in *Spirula*. Thus, the single-layer nature indicated by Mutvei (1972, 1997) is due to the amalgamation of the individual membranes. All in all, except for the 'chalky' layer of the connecting ring, which is absent in *Spirula*, and taking into account the difference in microstructure of the septal extension of the septal neck (nacreous in *Nautilus* and lamello-fibrillar in *Spirula*), the components of the *Nautilus* siphuncle (nacre and pillar layers, fibrous prismatic deposits of the septal neck, and organic membranes of the connecting ring) can be homologized to those of *Spirula* (Fig. 9). A deeper insight might be obtained on properly fixed material of *Nautilus*.

The siphuncle of *Sepia* consists merely of a densely laminated organic layer which distributes over the siphuncular zone of the cuttlebone (Bandel and Boletzky 1979; Checa et al. 2015). It is oblique to the septa and closes the adoral ends of the chambers (Fig. 9). We cannot decide whether this layer is homologous to the organic membrane complex of the connecting rings of *Spirula* and *Nautilus* (Fig. 9). The interior of the chambers of the cuttlebone contain vertical pillars (i.e. perpendicular to the septa) and horizontal membranes (Fig. 9). The pillars have complex fluted morphologies and are formed by the mineralization of an organic precursor (Checa et al. 2015). Bandel and Boletzky (1979) claimed that the *Sepia* pillars are homologous to those of *Nautilus* and *Spirula*, but both their different placement and mode of formation prevent any homology.

Model for chamber formation

A model for chamber formation can be reconstructed from the present and former evidence. Additional help comes from present models of chamber formation in ectocochleates: ammonoids and nautiloids (Klug et al. 2008; Klug and Hoffmann 2015).

After formation of the septum, the soft body translocates to produce a new chamber (Fig. 10a1, a2). Removal of the cameral liquid of the freshly formed chamber initiates before (as in *Nautilus;* Ward 1981) or at the same time that soft body translocation begins (Fig. 10a1). The rear soft body has the aspect of a sac replicating the shapes of the septal and siphuncular structures. Only the siphuncular mantle increases in length, whereas the shell and septum-producing mantle advance forward. Bandel (1982) and Bandel and Stinnesbeck (2006) described a dorsal attachment scar on the inside of the chamber corresponding to the main retractor muscle. Although they described it as a continuous ribbon, it is not totally clear if the muscle migrated progressively or detached and reattached between soft body translocation.

During forward movement of the body, shell wall production begins with the extrusion of the periostracum from the shallow periostracal groove (Fig. 10b). Immediately after, secretion of the outer and inner shell walls starts (Fig. 10c1). While the latter reaches its maximal thickness soon (at the position of the last-formed septum), the outer shell wall increases in thickness toward more initial chambers (compare Fig. 10c1 with Fig. 10d4), i.e. it continues to grow during the animal's entire life. This is possible because, contrary to the inner shell wall, it is permanently in contact with the soft tissue enclosing the shell (Fig. 2b).

When the position of the new septum is going to be reached, the adorally curved (convex) margin of the dorsal and lateral rear mantle begins to produce similarly shaped organic membranes (Fig. 10d1, d2). The spacing between the membranes becomes progressively reduced as the rear mantle progression speed diminishes. When mantle speed reaches a minimum, septum production begins with the secretion of closely spaced organic membranes (Fig. 10a3, d3). These self-organize through liquid crystallization along the whole surface of the septum and the septal neck. Concomitant with the early stage of septum secretion, more to the apex, the siphuncular mantle adheres to the septal neck of the preceding septum and begins to produce spaced organic membranes and pillars (Fig. 10e1, e2). These grow from the internal surface of the previous septal neck toward the interior. Pillar growth stops at some point before secretion of the organic membranes is complete, and the mantle produces a gel-like mineralizing extrapallial fluid, particularly in the area close to the septal neck (Fig. 10e3). Fibrous-prismatic deposits begin to crystallize after the mantle has abandoned their position. Connecting ring formation ends with the completion of the whole suite of organic membranes and of the fibrous prismatic deposits, which do not reach the more internal membranes (Fig. 10e4).

Once the chamber is closed and most of the cameral liquid is removed, the space between the dorsal apical septal surface and the inner shell wall begins to be mineralized by secondary deposits precipitated from residual cameral liquid trapped in this acute space by surface tension, with the formation of the adapical ridge (Fig. 10a2–a4, d4). In this way, the loose membranes left behind by the mantle before initiation of the septum become partly mineralized. In some cases, these deposits extend to the inner shell wall and cause secondary growth of the internal ends of the affected prisms (Fig. 10d4). This process does not happen in the ventral side of the chamber where the septal surface is parallel to the shell wall (e.g. Figure 7a), and there is no adequate space for cameral liquid retention.

When septum secretion is complete, the septal mantle detaches from the fresh septum, and forward advancement of the soft body resumes. The mantle area implicated in the secretion of the adoral septal edge suddenly changes from secreting septal material to secreting inner shell wall material. This is deposited below the adoral septal bevel, with the

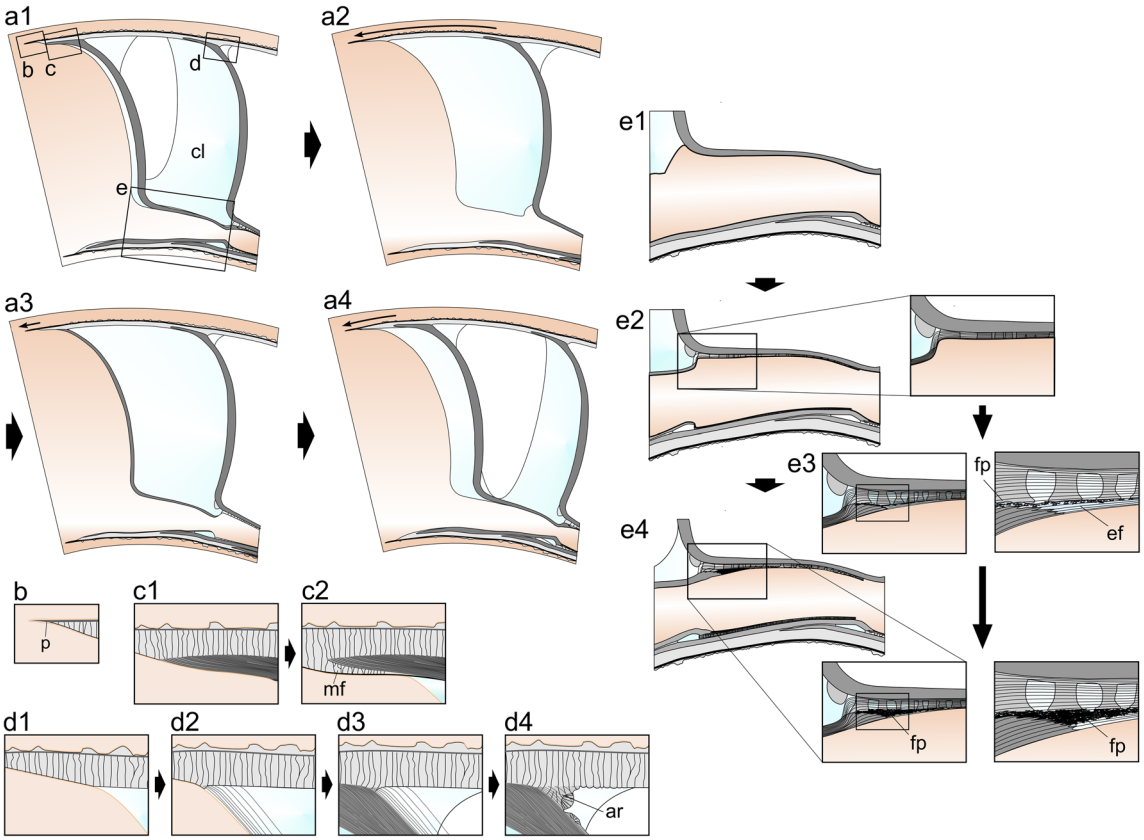

Fig. 10 Model for the chamber formation cycle and secretion of the shell structures in *Spirula*. **a1**–**a4** General chamber formation cycle. **a1** After formation of the septum and associated septal neck and connecting ring, the soft body advances at the same time as it introduces cameral liquid (cl) in the increasing cameral space. Drainage of cameral liquid of the newly finished chamber begins prior or at the same time, and previous chambers still retain remains of cameral liquid due to surface tension. **a2** The soft body advances to the position of the new septum. **a3** Secretion of a new septum. **a4** Septum secretion is finished, the soft body advances to the position of the new septum, and removal of cameral liquid is in process. In this way, the chamber formation cycle is finished. The positions of the structures described in **b**–**e** are indicated. Arrows in **a2**–**a4** indicate displacement of the soft body from the preceding stage. The cycle in **a1**–**a4** contemplates a vertical aperture, while the actual life orientation demonstrates an approximately horizontal aperture. According to the observations on living specimens, it is unclear whether the orientation is with the aperture looking downward (Schmidt 1922) or upward (Lindsay et al. 2020), or is changing. Lindsay's et al. observations seem particularly reliable since they were done on a free-living specimen, while Schmidt observed captive animals. The cameral liquid has been tentatively distributed assuming an upward-looking aperture. **b** Shell formation is initiated with the secretion of the periostracum (p) within the periostracal groove. Slightly after, formation of the inner shell wall begins. Initiation of the outer shell wall proceeds at a much slower pace. **c1**, **c2** Formation of the adoral septum edge and the mural flap (mf). **c1** The septum edge is finished, and its internal boundary is continuous with that of the shell wall edge. **c2** The mantle responsible for the secretion of the septal edge changes to a new secretion regime, to secrete the mural flap, which is identical in nature to the inner shell layer. While the inner shell layer soon reaches its maximal thickness, the outer shell layer, permanently surrounded by the soft body, increases in thickness toward the internal whorls; compare to thickness in **d4**. **d1**–**d4** Secretion of the apical septal edge and adapical ridge (ar). **d1**–**d2** When the mantle is close to the position of the new septum, its speed of advance becomes progressively reduced, and gradually closer organic membranes are secreted. **d3** Secretion of the septum is finished. The mantle has advanced beyond the adoral septum surface to create a new chamber (as in stages **a1** and **a4**). Cameral liquid is retained at the acute angle between the apical septal side and the shell. **d4** The adapical ridge is formed by precipitates derived from the residual cameral liquid. Additional calcified layers extend onto the apical septal surface and secondary growth of the prisms of the outer shell layer also takes place. The non-calcified areas of the organic membranes extending into the chamber are not preserved. **e1**–**e4** Formation of the connecting ring of the siphuncle. **e1** The mantle attaches to the septal neck of the previous septum. **e2** The pillar layer and the organic membranes extending from the septal neck are produced (see also close-up). **e3** Pillar production stops and a mineralizing extrapallial fluid (ef) is secreted. After the mantle has advanced for the production of new organic membranes, fibrous prismatic deposits (fp) begin to crystallize within the extrapallial fluid between the organic membranes. **e4** Completion of the connecting ring. The production of organic membranes ceases and the extrapallial fluid mineralizes completely. Note that the fibrous prismatic deposits do not reach the interstices of the most internal organic membranes

resulting formation of the mural flap (Fig. 10c2), both in the dorsal and ventral areas (this is a much more acute wedge). In this way, the chamber formation cycle is completed.

Supplementary Information The online version contains supplementary material available at https://doi.org/10.1007/s00227-022-04120-0.

Acknowledgements Serge Gofas (Dept. of Animal Biology, University of Málaga, Spain), Luis Sánchez-Tocino (Department of Biology, University of Granada, Spain), and Mercedes Checa-Ros (Department of Mineralogy and Petrology, University of Granada, Spain) provided shells. Vicente Hernández-García (Instituto Universitario EcoAqua, University of Las Palmas de Gran Canaria, Spain) procured the ethanol-fixed complete specimens. Funding was provided by projects PID2020-116660GB-I00 of the Spanish Ministerio de Ciencia e Innovación (AGC, CG, CS), and B-RNM-265-UGR18 of the Consejería de Conocimiento, Investigación y Unversidad of the Junta de Andalucía (AC), the Unidad Científica de Excelencia UCE-PP2016-05 of the University of Granada (AGC, CG), and the Research Group RNM363 of the Junta de Andalucía (AGC, CG).

Author contributions AGC: conceived and designed the study, acquired and analyzed data, wrote the paper. CG, EG, WWS, JHEC, CS, and MO: acquired and analyzed data and revised the paper.

Funding Open Access funding enabled and organized by Projekt DEAL.

Availability of data and materials Data are available from the authors on request.

Code availability Not applicable.

Declarations

Conflict of interest Authors do not have any conflict of interest.

Ethics approval Not applicable.

Consent to participate All authors agree on their participation on this paper.

Consent for publication All authors agree to be co-authors in the order submitted.

References

Appellöf A (1893) Die schalen von *Sepia*, *Spirula* und *Nautilus*: Studien über den Bau und das Wachstum. Kongl Svensk Vetensk Akad Handl 25:1–106

Bandel K (1982) Morphologie und Bildung der frühontogenetischen Gehäuse bei Conchiferen Mollusken. Facies 7:1–198. https://doi.org/10.1007/BF02537225

Bandel K (1990) Cephalopod shell structure and general mechanisms of shell formation. In: Carter JG (ed) Skeletal biomineralization, patterns, processes and evolutionary trends, vol 1. Van Nostrand Reinhold, New York, pp 97–115. https://doi.org/10.1029/SC005p0097

Bandel K, Boletzky S (1979) A comparative study of the structure, development and morphological relationships of chambered cephalopod shells. Veliger 21:313–354

Bandel K, Stinnesbeck W (2006) *Naefia* Wetzel 1930 from the Quirikina Formation (Late Maastrichtian, Chile): relationship to modern *Spirula* and ancient Coleoidea (Cephalopoda). Acta Univ Carolinae 49:21–32

Barskov S (1973) Microstructure of the skeletal layers of *Sepia* and *Spirula* compared with the shell layers of other mollusks. J Paleontol 3:285–294

Bøggild OB (1930) The shell structure of the mollusks. Kgl Dansk Vidensk Selsk Skrif Naturvidensk Math 9:231–326

Bouligand Y (1972) Twisted fibrous arrangements in biological materials and cholesteric mesophases. Tissue Cell 4:189–217. https://doi.org/10.1016/S0040-8166(72)80042-9

Carter JG, Bandel K, de Buffrénil V, Carlson SJ, Castanet J, Crenshaw MA, Dalingwater JE, Francillon-Vieillot H, Géraudie J, Meunier FJ, Mutvei H, Ricqlès A, de Sire JY, Smith AB, Wendt J, Williams A, Zylberberg L (1990) Glossary of skeletal biomineralization. In: Carter JG (ed) Skeletal biomineralization, patterns, processes and evolutionary trends, vol 1. Van Nostrand Reinhold, New York, pp 609–671. https://doi.org/10.1002/9781118667279.oth1

Carter JG, Harries PJ, Malchus N, Sartori AF, Anderson LC, Bieler R, Bogan AE, Eugene Coan EV, Cope JCW, Cragg SM, Garcia-March JR, Hylleberg J, Kelley P, Kleemann K, Kříž J, McRoberts C, Mikkelsen PM, Pojeta J Jr, Skelton PW, Temkin I, Yancey T, Zieritz A (2012) Illustrated glossary of the Bivalvia: treatise online, part N, Revised, Chapter 31, vol 1. Kansas University Paleontological Institute, Lawrence, pp 1–209. https://doi.org/10.17161/to.v0i0.4322

Cartwright JHE, Checa AG (2007) The dynamics of nacre self-assembly. J R Soc Interface 4:491–504. https://doi.org/10.1098/rsif.2006.0188

Checa AG, Rodríguez-Navarro AB (2001) Geometrical and crystallographic constraints determine the self-organization of shell microstructures in Unionidae (Bivalvia: Mollusca). Proc R Soc B 268:771–778. https://doi.org/10.1098/rspb.2000.1415

Checa AG, Cartwright JHE, Sánchez-Almazo I, Andrade JP, Ruiz-Raya F (2015) The cuttlefish *Sepia officinalis* (Sepiidae, Cephalopoda) constructs cuttlebone from a liquid-crystal precursor. Sci Rep 5:11513. https://doi.org/10.1038/srep11513

Dauphin Y (1976) Microstructure des coquilles de céphalopodes. I. *Spirula spirula* L. (Dibranchiata, Decapoda). Bull Mus Natl Hist Nat 3ème sér 382. Sci Terre 54:197–238

Dauphin Y (1977) Microstructure et flottabilité chez la spirule (Cephalopoda). C R Acad Sci Paris D 284:2483–2485

Doguzhaeva L (1996) Two early Cretaceous spirulid coleoids of the north-western Caucasus: their shell ultrastructure and evolutionary implications. Palaeontology 39:681–707

Doguzhaeva LA (2000) The evolutionary morphology of siphonal tube in Spirulida. Rev Paléobiol 8:83–94

Erben HK (1972) Uber die Bildung und das Wachstum von Perlmutt. Biomineralization 4:15–46

Fuchs D (2006) Fossil erhaltungsfähige Merkmalskomplexe der Coleoidea (Cephalopoda) und ihre phylogenetische Bedeutung. Berliner Paläobiol Abh 8:1–115

Fuchs D, Keupp H, Trask P, Tanabe K (2012) Taxonomy, morphology and phylogeny of late cretaceous spirulid coleoids (Cephalopoda) from Greenland and Canada. Palaeontology 55:285–303. https://doi.org/10.1111/j.1475-4983.2011.01125.x

Fuchs D, Iba Y, Ifrim C, Nishimura T, Kennedy WJ, Keupp H, Stinnesbeck W, Tanabe K (2013) *Longibelus* gen. nov., a new Cretaceous coleoid genus linking Belemnoidea and early Decabrachia. Palaeontology 56:1081–1106. https://doi.org/10.1111/pala.12036

Grégoire C (1961) Sur la structure de la nacre septale de Spirulidae, étudiée au microscope eléctronique. Arch Int Physiol Biochim 69:374–377. https://doi.org/10.3109/13813456109092805

Griesshaber E, Checa AG, Salas C, Hoffmann R, Neuser R, Walter P, Immenhauser A, Schmahl WW (2022) Form and function: architecture and skeletal element structure of the endoskeleton of the mollusk cephalopod *Spirula spirula* (Cephalopoda). Submitted

Hoffmann R, Reinhoff D, Lemanis R (2015) Non-invasive imaging techniques combined with morphometry: a case study from *Spirula*. Swiss J Palaeontol 134:207–216. https://doi.org/10.1007/s13358-015-0083-0

Hoffmann R, Lemanis RE, Wulff L, Zachow S, Lukeneder A, Klug C, Keupp H (2018) Traumatic events in the life of the deep-sea cephalopod mollusc, the coleoid *Spirula spirula*. Deep Sea Res I 142:127–144. https://doi.org/10.1016/j.dsr.2018.10.007

Klug C, Hoffmann R (2015) Ammonoid septa and sutures. In: Klug C, Korn D, De Baets K, Kruta I, Mapes R (eds) Ammonoid paleobiology: from anatomy to ecology. Topics in geobiology, vol 43. Springer, Dordrecht, pp 45–90. https://doi.org/10.1007/978-94-017-9630-9_3

Klug C, Meyer EP, Richter U, Korn D (2008) Soft-tissue imprints in fossil and recent cephalopod septa and septum formation. Lethaia 41:477–492. https://doi.org/10.1111/j.1502-3931.2008.00100.x

Klug C, Landman NH, Fuchs D, Mapes RH, Pohle A, Guériau P, Reguer S, Hoffmann R (2019) Anatomy and evolution of the first Coleoidea in the Carboniferous. Commun Biol 2:280. https://doi.org/10.1038/s42003-019-0523-2

Lemanis R, Stier D, Zlotnikov I, Zaslansky P, Fuchs D (2020) The role of mural mechanics on cephalopod palaeoecology. J R Soc Interface 17:20200009. https://doi.org/10.1098/rsif.2020.0009

Lindsay DJ, Hunt JC, McNeil M, Beaman RJ, Vecchione M (2020) The first in situ observation of the ram's horn squid *Spirula spirula* turns "common knowledge" upside down. Diversity 12:449. https://doi.org/10.3390/d12120449

Mutvei H (1964) On the shells of *Nautilus* and *Spirula* with notes on the shell secretion in non-cephalopod molluscs. Ark Zool 16:221–278

Mutvei H (1972) Ultrastructural studies on cephalopod shells. Part I. The septa and siphonal tube in *Nautilus*. Bull Geol Inst Univ Uppsala N Ser 3(8):237–261

Mutvei H (1997) Siphuncular structure in Ordovician endocerid cephalopods. Acta Palaeontol Pol 42:375–390

Mutvei H (2016) Siphuncular structure in the extant *Spirula* and in other Coleoids (Cephalopoda). GFF 139:129–139. https://doi.org/10.1080/11035897.2016.1227364

Mutvei H, Donovan DT (2006) Siphuncular structure in some fossil coleoids and recent *Spirula*. Palaeontology 49:685–691. https://doi.org/10.1111/j.1475-4983.2006.00533.x

Mutvei H, Dunca E, Weitschat W (2010) Siphuncular structure in the recent *Nautilus*, compared with that in Mesozoic nautilids and ammonoids from Madagascar. GFF 132:161–166. https://doi.org/10.1080/11035897.2010.510204

Neville AC (1993) Biology of fibrous composites. Cambridge University Press, Cambridge, UK

Oudot O, Neige P, Shir IB, Schmidt A, Strugnell JM, Plasseraud L, Broussard C, Hoffmann R, Lukeneder A, Marin F (2020) The shell matrix and microstructure of the Ram's Horn squid: molecular and structural characterization. J Struct Biol 211:107507. https://doi.org/10.1016/j.jsb.2020.107507

Schmidt J (1922) Live specimens of *Spirula*. Nature 110:788–790. https://doi.org/10.1038/110788a0

Ubukata T (1994) Architectural constraints of the morphogenesis of prismatic structures in Bivalvia. Palaeontology 37:241–261

Ward P (1981) The chamber formation cycle in *Nautilus macromphalus*. Paleobiology 7:481–493